NMR Structural Characterization of the Reaction Product between d(GpG) and the Octahedral Antitumor Complex *trans*-$RuCl_2(DMSO)_4$†

Gennaro Esposito,‡ Sabina Cauci,*,‡ Federico Fogolari,‡ Enzo Alessio,§ Marco Scocchi,‡ Franco Quadrifoglio,‡ and Paolo Viglino‡

Department of Biomedical Sciences and Technologies, University of Udine, Udine, Italy, and Department of Chemical Sciences, University of Trieste, Trieste, Italy

Received December 19, 1991; Revised Manuscript Received April 17, 1992

ABSTRACT: The reaction between the antitumor octahedral complex *trans*-$RuCl_2(DMSO)_4$ and d(GpG) leads to the formation of a stable compound characterized by a covalent bifunctional coordination of the bases to the metal center. The structure of the compound has been fully characterized by NMR and molecular modeling studies, showing the presence of two N7-coordinated guanine moieties in a head to head conformation, two dimethyl sulfoxide molecules, and one halogen atom in the coordination sphere of the ruthenium. The glycosidic χ angles are essentially in the anti range, the sugar puckering of the 5'G is 3'-endo (100% N), whereas that of the 3'G is more flexible but mainly in 2'-endo conformation (85% S), the two bases are strongly destacked. The compound shows structural features which are surprisingly similar to those exhibited by the corresponding cisplatin complex, indicating that such a way of interaction with DNA is not exclusive to Pt or to metals with square planar coordination geometries.

In recent years metal-based antitumor drugs have been playing a relevant role in antiblastic chemotherapy; especially *cis*-diamminedichloroplatinum (cisplatin or *cis*-DDP)[1] is regarded as one of the most effective anticancer drugs used in clinics (Loehrer & Einhorn, 1984; Muggia, 1991). In the design of new anticancer agents, different complexes of Pt-(II) (square planar) and of Pt(IV) (octahedral) were tested (Sherman & Lippard, 1987; Johnson et al., 1989; Chaney et al., 1991) and some of them are currently used in clinical applications (Twelves et al., 1991; Weiss et al., 1991). Among non-platinum transition metal anticancer compounds, ruthenium complexes (Clarke, 1989; Garzon et al., 1987) have raised great interest. In particular ruthenium(II) (Alessio et al., 1987; Sava et al., 1989) and ruthenium(III) (Pacor et al., 1991) complexes, with dimethyl sulfoxide (DMSO) as ligand, exhibit antiblastic activity comparable to that of cisplatin at equitoxic dosage in animal models of metastasizing tumors, but with less severe side effects and prolonged host survival times.

The mechanism of antitumor action of metal compounds is not fully understood, but in the case of the square planar cisplatin, a lot of experimental evidence points to DNA binding as the crucial lesion (Sherman & Lippard, 1987; Johnson et al., 1989). The bifunctional binding to adjacent purine bases d(GpG) or d(ApG), which represent 65% and 25% of total platinum binding (Fichtinger-Schepman et al., 1985), respectively, is widely accepted as the critical interaction with DNA, inhibiting replication and transcription processes (Sherman & Lippard, 1987; Johnson et al., 1989).

NMR (Sherman & Lippard, 1987; Girault et al., 1982; Reedijk, 1987; Mukundan et al., 1991) and X-ray investigations (Sherman et al., 1985; Admiraal et al., 1987) have been carried out in the last decade to elucidate the structural features of the interaction. The purine N7 bifunctional binding determines the loss of stacking in coordinated bases and leads to a bending of the double-helical DNA (Sherman & Lippard, 1987; Reedijk, 1987) associated to some extent with unwinding (Bellon et al., 1991).

The nature of DNA interaction with octahedral metal complexes has been much less explored. Attention has been focused on a ruthenium(II) complex [*trans*-$RuCl_2(DMSO)_4$], which exhibits interesting antiblastic activity and reacts in vitro and in vivo with DNA (Alessio et al., 1987; Mestroni et al., 1989; Cauci, 1990). This octahedral transition metal complex shows a mechanism of reaction similar to that of cisplatin, in spite of the different geometry, the N7 of the guanine bases being the preferential site of attack on DNA (Mestroni et al., 1989; Cauci, 1990). The reaction of *trans*-$RuCl_2(DMSO)_4$ with 5'-dGMP leads to the formation of two diastereoisomeric monoadducts in which the guanine moiety and the α-phosphate group form a chelate to the metal center with opposite chirality (Alessio et al., 1989). In the case of the reaction with 2'-dGuo an equilibrium state is achieved, two diastereoisomeric monoadducts and a biadduct being present in the reaction mixture. In all the cases the purine moiety is coordinated via N7 (Cauci et al., 1991). NMR evidence supports a head to tail arrangement of guanine moieties in the biadduct in analogy with corresponding adducts of square planar Pt(II) (Bau & Gellert, 1978) and Pt-(IV) (Choi et al., 1988) compounds.

The reversibility of monofunctional N7 purine coordination is in contrast with the irreversibility of binding to polymeric DNA (Cauci, 1990), strongly suggesting that a bifunctional binding occurs in the latter case. Therefore the dinucleotide d(GpG) was chosen as a better model to study the interaction of *trans*-$RuCl_2(DMSO)_4$ with nucleic acids. To our knowl-

† This investigation was supported by Italian CNR (Grant 9002985CT04) and MURST (60%).

* Address correspondence to this author: Department of Biomedical Science and Technologies, University of Udine, via Gervasutta 48, 33100 Udine, Italy.

‡ University of Udine.

§ University of Trieste.

[1] Abbreviations: *cis*-DDP, cisplatin or *cis*-diamminedichloroplatinum-(II); DMSO, dimethyl sulfoxide; 5'-dGMP, 5'-deoxyguanosine monophosphate; 2'-dGuo, 2'-deoxyguanosine; HPLC, high-performance liquid chromatography; CD, circular dichroism; TOCSY, total correlation spectroscopy; DQF-COSY, double-quantum-filtered correlation spectroscopy; NOESY, nuclear Overhauser effect spectroscopy; PIPES, 1,4-piperazinediethanesulfonic acid; MD, molecular dynamics; sugar phosphate torsion angles, P-α-O5'-β-C5'-γ-C4'-δ-C3'-ϵ-O3'-ζ-P; glycosyl torsion angle, O4'-C1'-χ-N9-C4.

0006-2960/92/0431-7094$03.00/0

edge, this is the first structural characterization of a covalent bifunctional coordination of an antitumor octahedral complex to d(GpG).

EXPERIMENTAL PROCEDURES

trans-$RuCl_2(DMSO)_4$ and *trans*-$RuBr_2(DMSO)_4$ were synthesized as previously reported (Alessio et al., 1988). d(GpG) sodium salt and other reagents were purchased from Sigma and used without further purification. A freshly prepared stock solution of the ruthenium complex in D_2O, typically 30 mM, was diluted to the desired final concentration. When necessary, the monohalogenated species was obtained by incubating the stock ruthenium solution for 8 h at 37 °C, in the dark, with equimolar $AgNO_3$, and then centrifuging to eliminate the AgCl formed.

HPLC analyses were performed on a Waters liquid chromatograph (equipped with a Model 680 automated gradient controller) on a μBondapack C_{18} reverse-phase column, with UV detection at 253 nm, using an aqueous 10 mM KCl solution as eluant A and CH_3OH as eluant B; the separation of the reaction products was achieved with a linear gradient from 0% to 20% B, at a flow rate of 1 mL/min.

CD spectra were acquired with a Jasco J600 dichrograph, equipped with a thermostated cell holder. UV spectra were recorded on the same samples with a Cary 2200 spectrophotometer whose cell holder was also thermostated.

NMR spectra were obtained at 500.13 MHz with a Bruker AM500 spectrometer. The temperature was adjusted at 23 °C in all the experiments except for the kinetic measurements (40 °C). Stoichiometric amounts of *trans*-$RuCl_2(DMSO)_4$ or *trans*-$RuBr_2(DMSO)_4$ were added, directly into the NMR tube, to d(GpG) solutions in D_2O (99.99% from Cambridge Isotope Laboratories). Typically the final concentration was 3.5 mM. In the titration experiments the pH (uncorrected reading) was adjusted by DCl or NaOD microadditions directly into the NMR samples. Twenty-four hours at 40 °C was sufficient to reach a nearly stationary composition of the reaction mixture. The final reaction product (A) was successively purified by HPLC and lyophilized before being redissolved in D_2O at 23 °C for further NMR studies (at a concentration typically of ≈1 mM). In these conditions, the samples were stable for over 2 weeks before oxidative degradation products could be detected.

All chemical shifts were referred to the free dimethyl sulfoxide resonance (2.73 ppm). Typical 1D spectral acquisition parameters were 5000-Hz sweep width, 1.64–3.28-s acquisition time, and 1–2-s relaxation delay. The map of the scalar coupling connectivities was obtained from the 2D TOCSY spectrum (Muller & Ernst, 1979) acquired using the pulse scheme proposed by Rance (1987) with a WALTZ 16 (Shaka et al., 1983) spin lock lasting 62.2 ms, at γB_2 = 7.7 kHz. Choosing the same spectral width in both dimensions (i.e., 5000 Hz), the acquisition times were 0.205 and 0.04 s in t_2 and t_1, respectively, i.e., a matrix 410 × 2K with 64 scans each t_1 increment. Zero filling to 2K was performed in t_1 prior to Fourier transformation. A square sine-bell function, shifted by $\pi/3$, was applied in both dimensions.

The high-resolution 2D scalar correlation map was obtained from a 2D DQF-COSY experiment (Piantini et al., 1982), acquired over a sweep width of 3205 Hz in both dimensions. This spectral window was selected to observe deoxyribose resonances unaffected by the folding in the spectrum of H8 lines. The acquisition times were 0.479 and 0.087 s, corresponding to a resolution of 2.1 and 11.4 Hz in t_2 and t_1, respectively. The experimental matrix (560 × 3K with 128 scans per t_1 increment) was zero filled to 4 × 4K, to achieve a final digital resolution of 1.6 Hz in both frequency domains, enough to allow for a detailed pattern attribution of the high-resolution (0.3 Hz) 1D spectrum employed for spin system simulation. A square cosine bell was used to condition the experimental data, in order to avoid spurious negative tails of the cross-peak patterns. No ^{31}P decoupling was performed. The simulations of the 1D patterns were performed separately for systems including nonlabile protons of each nucleoside moiety as well as the phosphorus nucleus. By means of the standard Bruker software program PANIC a satisfactory fitting of the experimental spectrum was obtained; in the worst conditions the probable parameter errors were 0.02–0.04 Hz, i.e., well below the experimental resolution.

Through-space connectivities were obtained by 2D NOESY experiment (Jeener et al., 1979), recorded at three different mixing times (t_m) (200.4, 419.3, and 858.7 ms), randomly varied (±5%) to minimize coherent transfers due to *J* couplings. 2D NOESY matrices were acquired with 128 scans for each of the 600 t_1 increments, over a sweep width of 5000 Hz in both dimensions (i.e., with a resolution of 4.9 and 16.7 Hz in t_2 and t_1, respectively). Zero filling to 2K was performed in t_1, and a square cosine-bell function was employed in both dimensions prior to 2D FT.

All 2D spectra were obtained with pure-phase line shapes using TPPI (Drobny et al., 1979) to achieve quadrature detection in t_1. The residual HOD resonance was always attenuated by coherent prolonged selective excitation (Esposito et al., 1987) with a DANTE scheme (Morris & Freeman, 1978) during the relaxation delay (typically 1.5–2.0 s) and the mixing time in NOESY experiments.

Molecular Modeling. A modified version of AMBER force field (Weiner et al., 1984) (see Table I) was used throughout the calculations. All the parameters employed were estimated on the basis of the literature (Mercer & Trotter, 1975; Alessio et al., 1988, (1992); Seddon & Seddon, 1984; Henn et al., 1991) on analogous compounds. As to the charges, these were calculated with the algorithm of Gasteiger and Marsili (1980) on a model compound including Ru, 2DMSO, Cl, H_2O, and the two N7's in order not to modify the AMBER parameters too heavily. Starting charges of +1, −1, and +0.5 were assigned to Ru, Cl, and N7, respectively. The final charges on the N7's were finally added to the original AMBER charges. The set of parameters involving the N7's and the sulfur atoms was duplicated and modified in order to parametrize differently cis and trans location relationships among the metal-attached atoms. No energy barrier was set for rotation about the bonds involving ruthenium.

The dynamic simulations were run for 1 ns in steps of 1 fs. Vacuum (ϵ = 1), water (ϵ = 80), and distance-dependent ($\epsilon = 4r$, with r in Å) dielectric constants were used for separate runs. The conformational space was searched for global minima using a constrained simulated annealing procedure (Kirkpatrick et al., 1983) starting dynamics at 930 °C, progressively reducing the temperature to −73 °C, and finally minimizing the energy of the resulting structures. A force constant of 100 kcal/mol·rad^2 was used in the constrained simulations.

RESULTS

The octahedral complex *trans*-$RuCl_2(DMSO)_4$ dissolved in water shows the dissociation mechanism reported in Scheme I. Two dimethyl sulfoxide molecules are released immediately after dissolution. The loss of the first chloride ion is observed after 6 h at 37 °C, whereas there is no evidence of release of

Table I: AMBER Force-Field Modifications[a]

bonds	K_r (kcal/mol·Å^2)	r_{eq} (Å)
S–O	528.0	1.48
Ru–S	400.0	2.30
Ru–O	400.0	2.14
Ru–N7	400.0	2.15
Ru–Cl	400.0	2.40
angles	K_θ (kcal/mol·deg^2)	θ_{eq} (deg)
Ru–C–S	70.0	112.0
Ru–S–O	70.0	119.0
–Ru–	100.0	90 or 180
Ru–N7–C8	100.0	128.1
Ru–N7–C4	100.0	128.1
Ru–O–H	100.0	109.5 (125)
dihedral angles	$V_\phi/2$ (kcal)	θ_{eq} (deg)
–Ru––*[b]	0.0	0.0
Ru–C4–N7–C8[c]	10.0	128.1
atoms	R (Å)	ϵ (kcal/mol)
Ru	2.0	0.200
Cl	2.0	0.200

[a] Following the notation of Weiner et al. (1984). The following charges (expressed in protonic charges) were used: Ru (+0.969), S (+0.115), O_{DMSO} (–0.258), C (+0.015), H_{methyl} (+0.036), H_{water} (+0.223), O_{water} (–0.509), Cl (–0.626), and N7 (+0.257). $E_{tot} = \sum_{bonds}K_r(r - r_{eq})^2 + \sum_{angles}K_\theta(\theta - \theta_{eq})^2 + \sum_{dihedrals}(V_\phi/2)[1 + \cos(n\Phi - \gamma)] + \sum_{i>j}\epsilon_{ij}[(r_{ij,eq}/r_{ij})^{12} - 2(r_{ij,eq}/r_{ij})^6] + \sum_{H\ bonds}[(C_{ij}/r_{ij}^{12}) - (D_{ij}/r_{ij}^{10})] + \sum_{i>j}(q_iq_j/\epsilon r_{ij})$. [b] $n = 0$. [c] $n = 2$.

the second chloride ion (Cauci et al., 1991). An enhancement of Cl^- release is induced by guanine moiety coordination to the metal center when *trans*-$RuCl_2(DMSO)_4$ is reacted with 2′-deoxyguanosine (Cauci et al., 1991).

When *trans*-$RuCl_2(DMSO)_4$ is incubated with d(GpG) at equimolar ratio (3.5 mM) in water at 40 °C (final pH 5.9), two different reaction products (A and B) are observed. Product B is an intermediate, which slowly disappears in about one day as shown in the kinetic pattern reported in Figure 1. At low temperature (≈5 °C), the conversion of the intermediate into the final product is strongly slowed down, thus allowing the HPLC separation and spectroscopic characterization of the compounds.

Product B exhibits dichroic bands much more intense than A (Figure 2). On the contrary, the final product A shows a negligible CD spectrum at pH 6 and a weak negative band (centered at about 280 nm) at alkaline pH values very similar to that exhibited by the corresponding complexes with cisplatin (Girault et al., 1982).

The aromatic region of the ^{1}H NMR, including the guanine H8 resonances recorded on the reaction mixture at 4 h, is reported in Figure 3. The large downfield shifts of the resonances arising from the final reaction product A (δ = 8.723 ppm and δ = 8.682 ppm) are typical of N7 coordination of guanine moieties to a transition metal center (Miller & Marzilli, 1985) and have been previously observed in the reaction of *trans*-$RuCl_2(DMSO)_4$ with 2′-dGuo (Cauci et al., 1991) and 5′-dGMP (Alessio et al., 1989). The two resonances at δ = 8.914 ppm and δ = 7.792 ppm, belonging to the intermediate product (B), cannot be attributed to a complex in which only one guanine is coordinated via N7 (vide infra). No monoadduct complex has indeed been observed in the investigated reaction.

A kinetic pattern similar to that of Figure 1 was observed when the reaction was carried out in buffered solution (30 mM PIPES, pH 7.5), all the other features being substantially unchanged except for the onset of a short-lived intermediate that disappears in the first 30 min. The nature of this intermediate has not been further investigated.

The pH titration of the reaction mixture in unbuffered water (Figure 4) clearly shows that in both the intermediate B and the final product A the ruthenium atom is coordinated via N7 atoms to two guanine moieties. In fact all the chemical shifts of the H8 are unaffected by lowering the pH below 4, contrary to what is expected for a free guanine N7 group (Girault et al., 1982), while at basic pH the relevant chemical shift changes observed are related to the decrease of the N1H pK_a, as previously found for the ruthenium dGuo complexes (Cauci et al., 1991) and N7 platinum complexes (Girault et al., 1982). On this basis we established that an N7, N7 chelated structure also occurs for the intermediate B. Moreover, the possibility of a phosphate coordination ca be easily excluded by analyzing the ^{31}P spectra, where the characteristic shift for a phosphate coordination at ruthenium (Alessio et al., 1989) was not observed.

From Figure 4 it can be seen that the H8 resonances of the intermediate B are shifted upfield at increasing pH values, as generally observed for the platinum complexes (Girault et al., 1982), while for the final product A the downmost resonance is shifted to lower field, probably due to ring current effects between the guanine residues.

The region of the ^{1}H NMR spectrum corresponding to DMSO methyl groups recorded on the reaction mixture shows up to eight resonances (depending on the pH value; see Figure 5) which can be assigned, on the basis of the kinetic profile, to the intermediate B and to the final product A. These assignments have been further confirmed by the NMR spectra of the HPLC isolated compounds. The number of resonances suggests a very low conformational mobility for DMSO ligands in the ruthenium complexes.

The pH dependence of the DMSO methyl chemical shifts is shown in Figure 5. The main feature of this profile is the coalescence at pH >10 of two methyl pairs of the final product A. This effect has not been observed for the intermediate product B, confirming the more asymmetric configuration of the latter compound. Parallel titration of the final product A by UV absorption indicates that the titration of the N1H groups of guanine moieties is spread over the range 6–10 of pH values (data not shown).

In order to verify the possible release of the Cl^- coordinated at the metal center, during both the incubation and the titration procedure, we incubated d(GpG) with *trans*-$RuBr_2(DMSO)_4$, whose behavior in water and with polymeric DNA is very similar to that of the corresponding chloride complex (Cauci, 1990). The kinetic pattern of the reaction in water at 40 °C proved to be very similar to that described for the *trans*-$RuCl_2(DMSO)_4$. However the H8 chemical shifts in the intermediate B′ (δ = 9.134 ppm and δ = 7.959 ppm) and the final product A′ (δ = 8.953 ppm and δ = 8.855 ppm) were slightly different compared to the corresponding values of products B and A. Both the titration patterns of CH8 and DMSO methyl resonances show a shift similar to that observed with the chloride but the individual values are different at each pH value, indicating that A, B, A′, and B′ are different compounds in the full pH range explored. This fact excludes, for all the compounds, the possibility of also losing the second halogen ligand at high pH values (in fact, the loss of the second halogen would render A = A′ and B = B′). Moreover, the absence of coalescence of the DMSO methyl pairs of A′ (Figure 6) seems to indicate a more constrained structure for the bromo derivative as expected because of the larger steric hindrance of the bromide ion. On the contrary, the release

Scheme I: Mechanism of the Reaction between *trans*-$RuX_2(DMSO)_4$ and d(GpG) in Unbuffered Water[a]

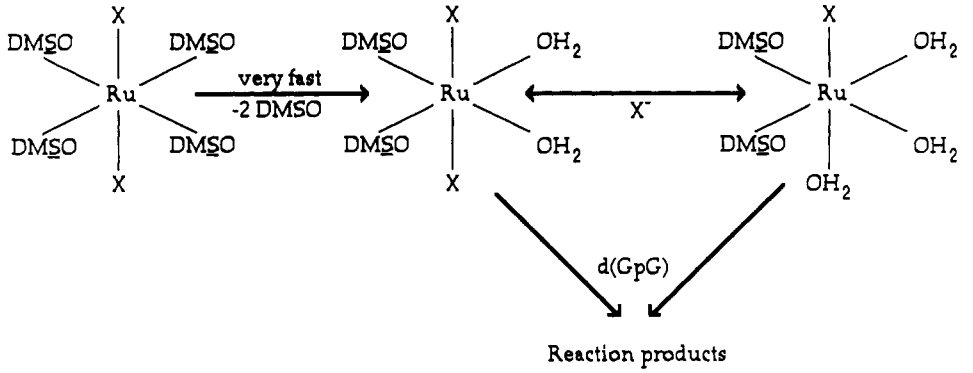

[a] N7, N7-coordinated guanine; DMSO, S-coordinated dimethyl sulfoxide; X = Cl, Br.

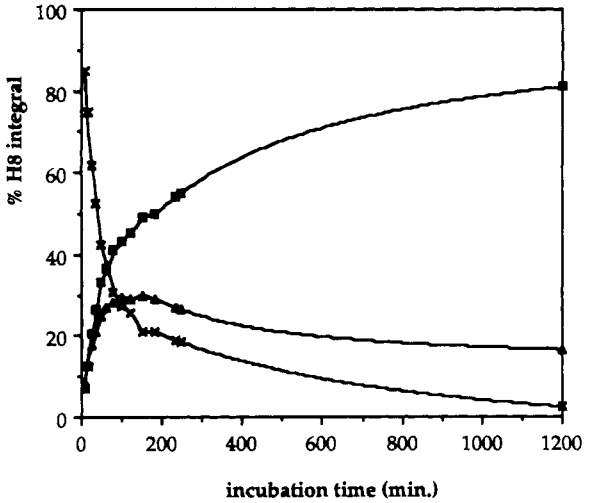

FIGURE 1: Time dependence of the concentration of different d(GpG) species in the reaction mixture: ⊡, complex A; ▲, complex B; ×, unreacted dinucleotide [d(GpG) dissolved in unbuffered water at equimolecular ratio with 3.5 mM *trans*-$RuCl_2(DMSO)_4$ at 40 °C]. The concentrations were determined by integration of the peak areas of the aromatic region [H8 of d(GpG)] in the ^1H NMR spectra.

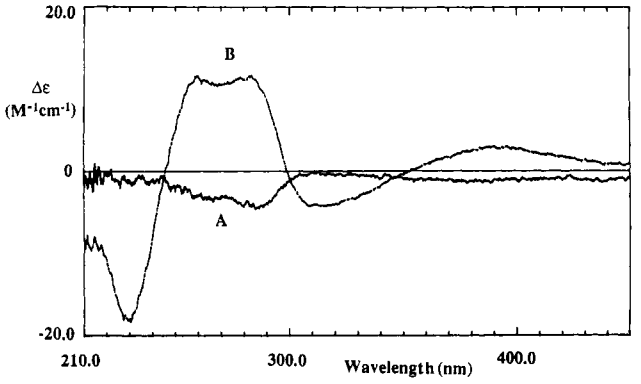

FIGURE 2: CD spectra of HPLC purified A and B reaction products in D_2O, pH 6.5, T = 23 °C.

of the first halogen ligand was confirmed by the reaction pattern obtained by incubating the dinucleotide with monohalogenated ruthenium species, which gave exactly the same reaction products.

The purified final reaction product A has been extensively studied by means of 1D and 2D NMR in order to elucidate its structure.

NMR Assignments. The examination of 2D TOCSY maps provided the connectivities within each deoxyribose spin system. The scalar networks were further confirmed by a 2D

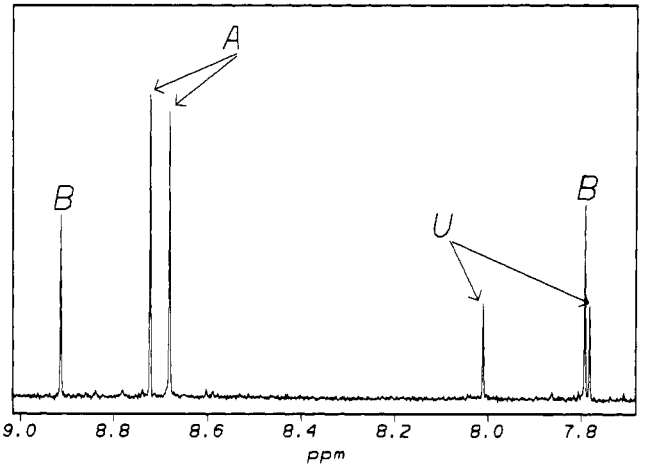

FIGURE 3: Low-field region of the ^1H NMR spectrum of the reaction mixture 4 h after dissolution of d(GpG) and *trans*-$RuCl_2(DMSO)_4$ in D_2O, at 40 °C. Guanine H8 resonances of the final (A), intermediate (B), and unreacted (U) are identified.

DQF-COSY spectrum that, in addition, allowed a proper attribution of the coupling pattern fine structure for subsequent 1D simulations (vide infra). Each sugar ring spin system was connected to the attached guanine via the H8 NOESY cross peaks to H2′ and H3′ resonances (Wuthrich, 1986). Additional base–sugar connectivities were consistent with the chosen attribution.

The detection of sequential contacts between the downmost H8 resonance and the deoxyribose H1′, H2′, and H2″ of the adjacent residue, while further supporting the attribution based on the intraresidue contacts, also gives the relative position of each residue in the sequence. Namely, the system with the downfield H8 resonance is the 3′-terminal residue and will henceforth be referred to as G2. Consistently, the 5′-terminal residue will be indicated as G1. These conclusions are also in line with the chemical shifts of the sugar spin systems, which are expected to exhibit a detectable difference for C5′ protons (esteric in G2 and alcoholic in G1). The assignment list is given in Table II.

Combined 2D NOESY and J-Coupling Analysis. The qualitative interpretation of the intraresidue NOESY correlations allows restriction of the conformational space for both residues. The intranucleotide very weak H8–H1′ contacts along with the stronger H8–H2′, H8–H2″, and H8–H3′ connectivities agree with a χ angle in the anti range (−90°/−170°) for both residues (Wuthrich, 1986). The latter contacts may also be indicative of the sugar puckering (Wuthrich, 1986). Indeed, the strong H8–H3′ cross peak observed for G1 suggests a N-type conformation of the corresponding deox-

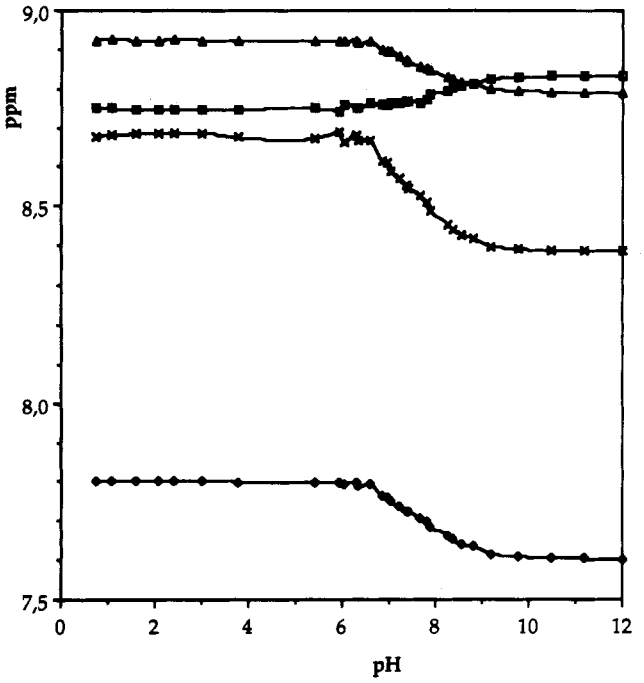

FIGURE 4: pH dependence of H8 chemical shifts of the products of the reaction between d(GpG) and *trans*-$RuCl_2(DMSO)_4$: ■, AI; ×, AII; ▲, BI; ● BII.

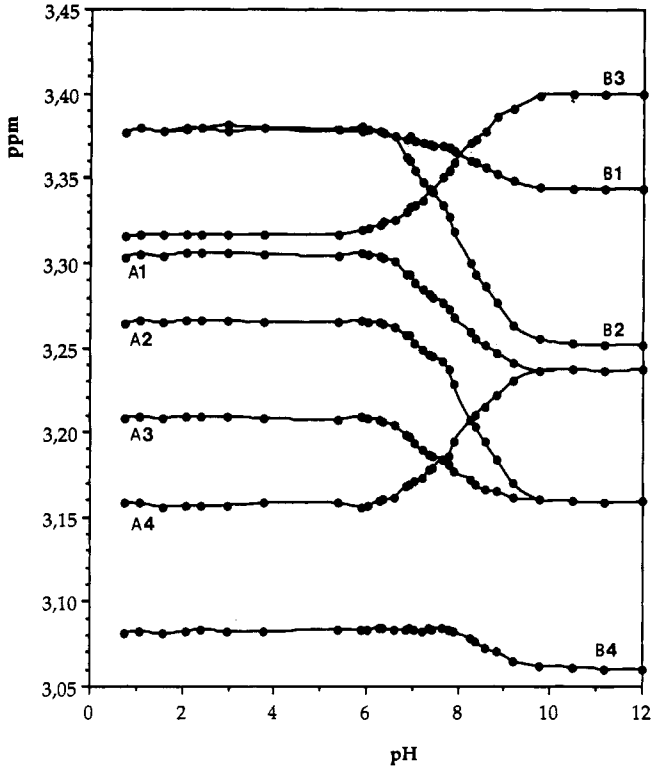

FIGURE 5: pH dependence of the chemical shifts of the DMSO methyl groups of the products of the reaction between d(GpG) and *trans*-$RuCl_2(DMSO)_4$.

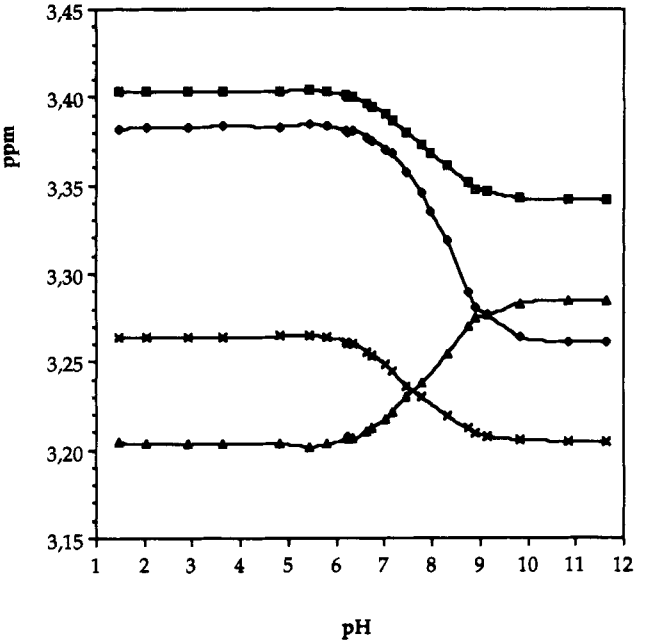

FIGURE 6: pH dependence of the chemical shifts of the DMSO methyl groups of the product A′ from the reaction between d(GpG) and *trans*-$RuBr_2(DMSO)_4$: ■ A′1; ◆, A′2; ×, A′3; ▲, A′4.

Table II: Comparison between Chemical Shifts (ppm) and Coupling Constants (Hz) of Compound A (This Work) and of d(GpG) with *cis*-DDP (den Hartog et al., 1982) (T = 23 °C, pH 6.5)

	chemical shifts			
proton	G1(A)	G2(A)	G1(*cis*-DDP)	G2(*cis*-DDP)
1′	6.251	6.330	6.186	6.222
2′	2.542	2.602	2.618	2.712
2″	2.812	2.480	2.735	2.556
3′	4.924	4.633	4.623	4.724
4′	4.122	4.207	4.073	4.229
5′	3.772	4.064	3.801	4.042
5″	3.834	4.114	3.520	4.042
8	8.659	8.753	8.267	8.572
	coupling constants			
couple	G1(A)	G2(A)	G1(*cis*-DDP)	G2(*cis*-DDP)
1′2′	0.9	9.0	0.6	8.1
1′2″	7.6	5.4	7.3	6.0
2′2″	−14.0	−13.6	−13.9	−13.6
2′3′	7.4	6.7	6.8	6.1
2″3′	10.8	2.9	10.7	2.9
3′4′	8.0	3.6	8.1	3.2
3′P	7.7	–	7.0	
4′5′	2.8	2.0	2.7	2.9[a]
4′5″	2.6	3.8	3.4	2.9[a]
4′P		1.8		2.8
5′5″	−13.1	−11.7	−12.8	
5′P		2.3		3.2[a]
5″P		3.5		3.2[a]

[a] In *cis*-DDP only the sum of the coupling constants 4′5′ + 4′5″ and 5′P + 5″P was obtained (den Hartog et al., 1982).

yribose. For G2 conflicting NOEs are observed, between H8 and C2′ and C3′ protons, that may arise from fluctuation of the sugar puckering phase angle and/or χ torsion angle, as well as from higher order effects affecting the intensity of dipolar connectivities (Kumar et al., 1981; Macura et al., 1981; Borgias & James, 1988). The unfavorable value of the molecular tumbling rate (≈0.2 ns) required the use of long mixing times in order to achieve a signal to noise ratio amenable to quantitation. Thus any approximate NOESY quantitative analysis based on the isolated spin pair and/or the initial linear buildup regime approximations (Kumar et al., 1981) proves affected by systematic underestimation of the interproton distances (Borgias & James, 1988). Nor would a complete relaxation matrix treatment of the NOESY data remove ambiguities in the presence of conformational equilibria not characterized in independent investigations.

The examination of the deoxyribose spin system coupling constants may help to remove ambiguity about G2 conformation and is expected also to add further quantitative details

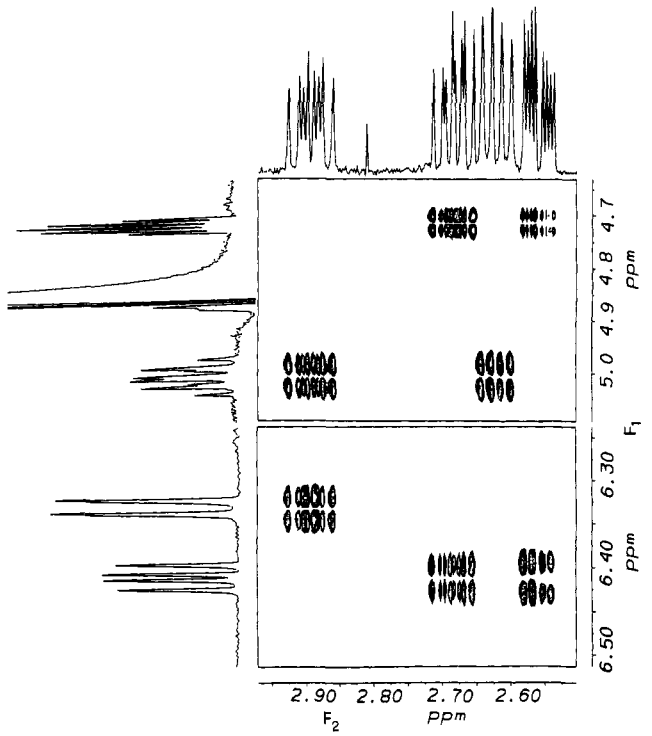

FIGURE 7: 500-MHz ^{1}H NMR 2D DQF-COSY spectrum of the final compound A as obtained, after purification, from the reaction between d(GpG) and *trans*-$RuCl_2(DMSO)_4$. The connectivities of deoxyribose 2′- and 2″-protons to 3′-(upper panel) and 1′-protons (lower panel) are shown. Positive and negative contour levels are plotted without distinction. The corresponding 1D spectrum traces are also reported. Inspection of the cross-peak antiphase pattern enables the detailed interpretation of the corresponding 1D multiplet fine structure, for subsequent quantitative refinements via least squares fitting of the simulated and experimental 1D pattern.

to the conformational features of G1 (Altona, 1982). Simulation of the coupling pattern in the 1D NMR spectrum for both sugar spin systems, including the heteronuclear couplings, led to the results listed in Table II. Qualitative inspection of the fine structure in 2D DQF-COSY cross peaks was sufficient for a detailed attribution of 1D splitting pattern (Figure 7). The J values are consistent with a pure N-type conformation for the G1 residue, whose P and ϕ_M, the pseudorotation angle and puckering amplitude (Saenger, 1984), were estimated to be ≈0° and 35°, respectively, according to the tables given by Rinkel and Altona (1987). At variance, no single conformation accounts for the observed J couplings in residue G2. The experimental values are therefore interpreted in terms of the equilibrium between the two most stable limit conformers N and S (Altona, 1982; Rinkel & Altona, 1987).

According to the equation reported by Altona (1982)

$$p(S) = [17.8 - (J_{1'2''} + J_{3'2''})]/10.9 \quad (1)$$

the percentage of G2 S conformer (p(S)) was 85% entailing some 15% in N conformation (as opposed to 100% N conformation evaluated for G1 with the same equation). The analysis of the J-coupling values of the H4′ with C5′ proton pair and the heteronuclear couplings ($J_{3'P}$ for G1 and $J_{4'P}$, $J_{5'P}$, and $J_{5''P}$ for G2) may be exploited to estimate the single γ_1, γ_2, ϵ_1, and β_2 (Altona, 1982). The J constants of G1 C5′ protons with the vicinal H4′ (Table II) are small and approximately equal (2.8 and 2.6 Hz). On the basis of the generalized Karplus equation (Karplus, 1959; Haasnot et al., 1980), one can argue that these values do not correspond to a single conformation, but rather to a restricted family of rotamers centered around $\gamma_1 \approx +60°$ (γ^+). An interpretation in terms of the three classical rotamers (γ_1 = +60°, 180°, –60°), using limit proper J values (Haasnot et al., 1980) leads to physically inconsistent results. This may be not unexpected when the rotational distribution is confined within a rather narrow width. Moreover, the asymmetry of the C4′H–C5′H_2 ethanoid fragment should be considered before choosing the "idealized" staggered rotamers. As suggested by Altona (1982), a reasonable assumption is to rely on the most commonly occurring γ values in oligonucleotides (γ^+ = 53°, γ^- = 70°, γ^+ = 180°).

In spite of this "judicious" choice, the idealized ternary model appears however unsatisfactory for describing the γ distribution in a double-helix structure with strong preference for γ^+ conformations. A rotational restriction imposed because of the very low occurrence of the γ^- conformation in DNA leads to (Altona, 1982)

$$p(\gamma^+) = [13.3 - (J_{4'5'} + J_{4'5''})]/9.7 \quad (2)$$

to estimate the amount of γ^+ rotamer. For our dinucleotide–ruthenium complex the rotational restraints acceptable for the DNA duplexes cannot be adopted tout court. First, even with the very small J constants of G1 C5′ protons, the bias for the rotational distribution of γ cannot be safely assessed without a preliminary stereospecific assignment of the 5′-geminal pair. In addition, the choice of the limit rotamers, i.e., the width of the rotational fluctuation, appears to drive the result of the calculation toward completely different distribution independent of the stereospecific assignment because of the very close values of $J_{4'5'}$ and $J_{4'5''}$. Namely, using the limit rotamers with γ = +53°, 180°, and –70°, one obtains $p(\gamma^+)$ = 83%, $p(\gamma^t)$ = 13–15%, $p(\gamma^-)$ = 2–4%, while for γ = 43°, 180°, and –64° one obtains $p(\gamma^+)$ = 90%, $p(\gamma^t)$ = 0%, $p(\gamma^-)$ = 10% [the sum relationship of eq 2 would give $p(\gamma^+)$ = 82%]. Apparently even more intriguing results are obtained for G2. Here the small $J_{4'5}$ values (2.0 and 3.8 Hz) again indicate the predominance of the γ^+ rotamers ($\gamma_2 \approx$ 60°), but the extraction of physically meaningful distribution depends on the stereospecific assignment for different sets of limit rotamers (Altona, 1982). The consideration of C5′ protons' NOEs may provide some clue for their stereospecific identification. In both the deoxyribose moieties the closest 3′–5′ contact is exhibited by the downfield C5′ proton. Unfortunately the reliability of these NOEs is partially reduced by strong coupling effects, expected because of the limited chemical shift difference of C5′ geminal pairs (≈0.5 ppm) (Kay et al., 1986). Thus, when both C5′ hydrogens are involved in NOE connectivities, as observed for G1, the relative intensities should be regarded with some care. Hence no firm conclusion can be reached for G1. On the contrary, the observation of a single intraresidue 3′–5′ contact in G2 suffices to assign stereospecifically the lowfield C5′ proton resonance as *pro-R* and allows the conclusion that γ_2 rotational distribution entails mainly γ^+ (82%) and γ^t (16%) conformers, choosing limit rotamers with γ = 43°, 180°, –64° (Altona, 1982) according to the commonly occurring distribution in oligonucleotides.

Incidentally, we also notice that the relative chemical shifts of *pro-R* and *pro-S* resonances do not agree with the usual occurrence reported for C5′ hydrogens (Remin & Shugar, 1972).

The stereospecific identification of G2 C5′ protons also enables an unambiguous evaluation of the β_2 torsion angle, using the $J_{5'P}$ and $J_{5''P}$ values (Table II) in the Lankorst et al.

equation (Lankorst et al., 1984):

$$J_{HCOP} = 15.3 \cos^2 \phi - 6.1 \cos \phi + 1.6 \quad (3)$$

where $\phi = \phi^R$ or ϕ^S, i.e., the H5''–C5'–O–P and H5'–C5'–O–P dihedral angles, being $\beta = \phi^R - 120° = \phi^S + 120°$. Calculations yield $\phi^S = \pm 60°, \pm 95°$ and $\phi^R = \pm 53°, \pm 102°$, that are compatible only for $\phi^S \approx +60°$ and $\phi^R \approx -53°$; i.e., $\beta_2 = -177 \pm 3°$. Overall a limited deviation from $\gamma^+\beta^t$ conformation seems to emerge for G2, which apparently conflicts with the value of the G2 long-range $J_{4'P}$ (1.8 Hz). Although no reliable parametrization of $J_{4'P}$ (γ, β) has been established yet, an average experimental value of 3.3 Hz has in fact been suggested by Altona (1982) for typical $\gamma^+\beta^t$. It is rather hard to evaluate the effect of a γ_2 fluctation on the value of $J_{4'P}$ without accounting for the accompanying β_2 rearrangement (the two torsion angles are interdependent). It seems interesting to note, however, that the amount of G2 γ^t rotamer (16%) is similar to the amount of G2 N-type conformer (15%), suggesting that γ_2 fluctations may be viewed within a molecular framework involving concerted rearrangement. Equation 3 can be employed also for evaluating ϵ_1 by exploiting the G1 $J_{3'P}$ coupling constant (Table II) and the relationship $\epsilon = \phi_{3'P} - 120°$. Among the four possibilities calculated from eq 3, only two are acceptable after ruling out the unfavorable ϵ^- conformers, i.e., $\epsilon_1 \approx -151°$ or $\epsilon_1 = +63°$. Inspection of a NOE restrained model leads to the retention of only the former value, i.e., $\epsilon_1 = -151°$, a conformation commonly encountered in RNA oligomers (Saenger, 1984) but reported also in alternating N–S oligodeoxyribonucleotides (Altona, 1982).

Once combined all together these structural elements can provide a model for the coordination complex of d(GpG) to ruthenium, which accounts also for the G1 H8–G2 H8 proximity inferred from the corresponding connectivities, observed in NOESY spectra. The presence of this contact clearly indicates a head to head arrangement of the two bases, coordinated at the central metal via N7, N7 chelation. Moreover the low asymmetry of the metal center as suggested by the CD spectrum (Figure 2) and the coalescence at basic pH of the DMSO methyl resonances (Figure 5), indicate that N7, N7 cis chelation of d(GpG) to ruthenium is accommodated in equatorial synclinal position, opposite to the DMSO ligands, with the axial positions still engaged in water and chloride coordination.

Molecular Modeling. Starting from the structural restraints discussed above, a preliminary investigation of the possible conformations of compound A was undertaken. As a starting model a complex between the two isolated nucleosides, i.e., without phosphate groups connecting the deoxyribose moieties, and $Ru(DMSO)_2$ via the N7's was chosen. The phosphate group, the Ru-coordinated water, and the chloride atom were added later. In this first step the charges on Ru and the DMSOs were taken equal to 0 while the AMBER parameters were left unchanged for the two nucleosides. The torsional angles were frozen at the following values:

$\chi_1 = -154°$ $\gamma_1 = 45.5°$ $\delta_1 = 84.3°$

$\chi_2 = -97.8°$ $\gamma_2 = 53.0°$ $\delta_2 = 156.4°$

which are close to the standard values for single-strand A- and B-DNA (Saenger, 1984) (entailing pure N and S deoxyribose ring puckering, respectively) and are in agreement with the experimental restraints. The two torsional angles defined by the sequence C8–N7–Ru–S, Θ_1 and Θ_2 for the respective residues, were then rotated in steps of 18° in order to get an energy map. The low-energy regions were further examined to check if the distance between the O5' and the O3' atoms was sufficiently short to accommodate a phosphate group with no major changes in the structural parameters. We were rather tolerant in this step since unfreezing the remaining degrees of freedom could reduce this distance. Such a procedure, while not expected to give a realistic energy quantitation, can nevertheless monitor steric hindrance, which energies by far overcome the inaccuracy of both the model and the force field. The only two regions that could match the above requirements were those centered around −108°, 108° and 108°, −108° in the Θ_1, Θ_2 plane, corresponding to head to head conformations which also fit well the experimentally observed proximity of the H8 protons.

Starting from these two conformations, the angles Θ_1, Θ_2, χ_1, and χ_2 were roughly adjusted in order to add the phosphate groups. We chose to add the water molecule on the side where a hydrogen bond could be possible with the O6 atoms of the base; the opposite choice would have brought the chloride atom in close contact with the same atoms. Once the satisfactory initial conformation was obtained, a preliminary constrained energy minimization in vacuo, to remove high-energy spots introduced in the previous step, was run using the complete modified AMBER force field. The following values were assumed to represent the experimental data:

$\gamma_1 = 45.5°$ $\delta_1 = 84.3°$ $\epsilon_1 = -151°$

$\beta_2 = 180°$ $\gamma_2 = 53.0°$ $\delta_2 = 156.4°$

In this way two starting structures for subsequent analysis were obtained. Since all the simulations do not take into account the solvent and a dielectric constant of 1 was used throughout, the energy differences between them at this level are not very significant.

For the structure corresponding to $\Theta_1 \approx 108°$ and $\Theta_2 \approx -108°$ [which will be called hereafter model 2, as opposed to the other called model 1 (Figure 8a) with $\Theta_1 \approx -108°$ and $\Theta_2 \approx 108°$], the addition of the phosphate group and the subsequent minimization led invariably to a loss of the anti conformation in one or both residues (in addition, the final conformer was also the one at higher energy).

In order to sample the conformational space around the two structures obtained, possibly overcoming energy barriers, we ran restrained simulated annealing for both conformations assuming alternatively $\epsilon = 1$ and $\epsilon = 80$. For both starting structures the choice of $\epsilon = 1$ led to results inconsistent with the experimental findings, due to the overestimated electrostatic interactions. The choice of $\epsilon = 80$, unrealistically reducing the electrostatic interactions, increases the accessibility of the conformational space sampling, which is highly desirable when the model does not include all the features of the system under investigation (like the interactions with the solvent). The results obtained in this case are different for the two starting structures. In none of the runs was the simultaneous presence of χ_1 and χ_2 in anti conformation found for model 2, thus confirming the probable inconsistency of this model with the experimental data. At variance for model 1, χ_1 is preserved in the anti range (close to −150°) in most of the runs while χ_2 varies within a large range of values including also anti conformations. The structural restraints, however, introduce a strong correlation among χ_2 and the backbone angles ζ and α which determine the orientation of the phosphate group relative to the complex (provided that

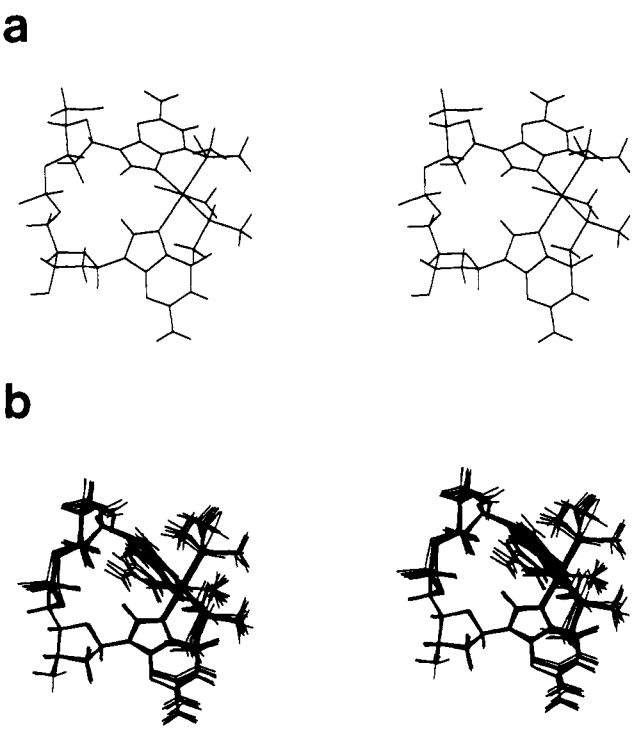

FIGURE 8: (a) Stereo drawing of the starting model of compound A (model 1); (b) superimposed stereo drawing of eight structures of compound A as obtained after simulated annealing.

the other angles are forced to their experimental values). Whenever the angle χ_2 is in the anti range, which happens in 20% of the runs, ζ and α both assume values close to –60°, forcing the phosphate oxygens outward with respect to the metal center, presumably toward the solvent. This arrangement is expected to occur in solution, where the phosphate group can be involved in hydrogen bonds with the water molecules. Incidentally, the values of ζ and α are those commonly occurring in the X-ray structure of nucleic acids. A stereoview of some of the superimposed final structures obtained is given in Figure 8b.

The variability of χ_2 can be ascribed to the very poor solvent representivity in conjunction with the type of restraints inferred from experimental data for residue G2, whose increased mobility should ultimately reflect a rather broad minimum in the conformational energy map.

The reliability of the class of structures originating from model 1 was further investigated. In particular an MD simulation was run at 27 °C, imposing a distance-dependent dielectric constant $\epsilon = 4r$ (r in Å). The results were rather striking since the overall features were also maintained when the experimental restraints were removed. The angles ϵ_1, β_2, and γ_2 stayed close to their experimental values. The endocyclic angles δ_1 and δ_2 are interesting since they should be sensitive to the sugar puckering and mobility. The results nicely agree with the picture of the G1 sugar ring fixed in N conformation (δ_1 = 84.3°) and G2 moving between N and S conformers (δ_2 = 156.4°), in agreement with the NMR analysis. The values of δ_2 were found to scatter between the two limit values, showing no preference for either of the two conformers.

The 5′-terminal CH_2OH is found, as expected from model inspection, completely free to rotate, thus contradicting the experimental data. Even accounting for an imperfect parametrization of the Karplus relationship in free 5′-terminals, the NMR inequivalence of G1 H5′ and H5″ (significantly increased on complexation) along with their small coupling constants to H4′ can hardly be reconciled with a free rotating 5′-terminal. According to the model, a hydrogen bond might be formed with an oxygen of the phosphate group (G1 O5–OP separation ≈3.0 Å). Water bridges with phosphate oxygen may also be responsible for blocking rotation around the C4–C5 bond.

In simulations with distance-dependent dielectric constant, χ_1 and χ_2 depart from their initial values and both vary around 180° in a range of approximately 40° so that they do not completely agree with the data. This behavior parallels the rearrangement of the angles ζ_1 and α_2, close, most of the time, to 60° and 180°, respectively. These values maintain, however, the phosphate group pointing outward.

In conclusion, the fair agreement between the simulations and the experimental findings strongly points to model 1 as the structure adopted by d(GpG)–$RuCl(DMSO)_2(H_2O)$ in solution.

Comparison of d(GpG) Conformation in Ruthenium and Platinum Complexes. In summary, the data discussed so far suggest that the spatial arrangement of d(GpG) complexed with ruthenium is closely related to the conformation it adopts in the *cis*-DDP complex, obtained via NMR studies (den Hartog et al., 1982) and successively confirmed by the X-ray structure of the cisplatin–d(pGpG) complex (Sherman et al., 1985). In the ruthenium complex the deoxyribose skeleton is rigid in G1, with a nearly pure N conformation, and more flexible in G2, with some 85% S-type and 15% N-type puckering equilibrium, as inferred from *J*-coupling analysis. The base–sugar relative orientations exhibit the same mobility difference, being anti in both nucleoside moieties, but with a much more reduced fluctuation amplitude in G1. The latter conclusion rests mainly on 2D NOESY evidence and on subsequent molecular dynamics simulations. Despite the systematic deviation expected in NOESY quantitative analysis from the assumption of the isolated spin-pair model, approximate distance restraints for G1 are compatible with only a limited range of χ_1 values, i.e., a limited class of closely related anti structures. At variance a much broader family of χ_2 conformations is obtained for G2, even constraining its sugar part in the most populated S conformer. No attempt was made to simulate the simultaneous fluctuation of G2 χ angle and deoxyribose puckering because of the inherent accuracy limits of our NOE quantitative determinations. An analogous G2 conformational freedom has been reported in the *cis*-DDP complex and was regarded as surprising by den Hartog and co-workers (1982), in view of the expectedly strict stereochemical requirements of a chelating dinucleotide. In both ruthenium and platinum adducts, the complexation of d(GpG) occurs via N7, N7 chelation with a head to head arrangement of the bases (den Hartog et al., 1982; Sherman et al., 1985). In a head to tail geometry G1 and (or) G2 O6 are intuitively expected to engage unfavorable steric and electrostatic interactions with the axial chloride, while both may be involved in hydrogen bonds with the opposite axial water molecule when one of the head to head arrangements is selected. This feature if further confirmed by the results of our simulations shown in Figure 8, where the distances H_{water}–O6 and O_{water}–O6 range between 1.83 and 3.09, and 2.61 and 2.78 Å, respectively. Thus no steric hindrance is found between guanine O6 and axial water. Whether and to what extent these interactions are actually responsible for the stabilization of a single diastereoisomer out of four possible it is hard to predict because of lack of information about the orientation of the bulky DMSO molecules.

As a matter of fact, in the chosen head to head geometry the values of Θ_1 and Θ_2 are very close to the corresponding angles derived from the X-ray structure of d(pGpG)–Pt (Sherman et al., 1985) using the definitions and the figures reported. The dihedral angle between the oriented planes of the bases, which is found around 100° in our starting model, varies within a large range (60–100°) in the structures obtained by simulated annealing. A similar unstacking of the bases has been reported for the cisplatin analog (76–87°) (Sherman et al., 1985).

As far as the remaining conformational features are concerned, ϵ_1 and β_2 dihedral angles are quite similar in the ruthenium and platinum complexes of d(GpG). In fact, for the *cis*-DDP complex a $\epsilon_1 = -162°$ has been evaluated (den Hartog et al., 1982; Sherman et al., 1985) in good agreement with the $\epsilon_1 = -151°$ of the ruthenium complex. The β_2 value in the cisplatin analog could not be safely assessed because of chemical shift equivalence of the G2 C5′ protons (den Hartog et al., 1982). The sum of their coupling constants to phosphorus was therefore employed to calculate the relative population of β^t conformer (93%). Complexation with ruthenium removes the chemical shift degeneracy of G2 C5′, protons and their stereospecific assignment allows a precise estimate of β_2 (−177°). This value corresponds to 96% β^t conformer, if stereospecific assignments are disregarded and limit rotameric populations are calculated, i.e., a conformational distribution very close to that observed with platinum.

Slightly different rotational distributions are observed for γ_1 and γ_2. In the d(GpG) cisplatin complex at 23 °C γ_1 and γ_2 exhibit an approximately equal population of most abundant γ^+ (77% and 79%, respectively), while with ruthenium the two distributions appear to be different (γ^+ = 83–90% for γ_1 and 82% for γ_2).

DISCUSSION

The octahedral antitumor complex *trans*-$RuCl_2(DMSO)_4$ is able to form a 1,2-intrastrand cross-link with d(GpG); preliminary measurements on d(TpGpGpT) indicate that a similar behavior can be extrapolated to higher molecular weight DNA. Moreover the presence of two N7-coordinated guanine moieties, two dimethyl sulfoxide molecules, and one halogen atom in the coordination sphere of the metal was demonstrated in both the intermediate and final reaction products.

The final reaction product shows structural features which are surprisingly similar to those exhibited by the corresponding cisplatin complex, indicating that such a way of interaction with DNA is not exclusive to Pt or to metals with square planar coordination geometry, as previously suggested (Lippard, 1987), but is probably a common motif in the interaction of transition metal complexes which possess two ligand positions in cis available for covalent binding. If one assume that the 1,2-intrastrand cross-link lesion on DNA is the crucial damage responsible for the antitumor effect, our findings can give the rationale to the design of octahedral metal based anticancer compounds.

NMR and molecular modeling studies depict a structure very similar to that described for *cis*-DDP, in which the bases have a head to head disposition, with the glycosidic χ angles essentially in the anti range, and the sugar puckering of 5′G is 3′-endo, whereas that of the 3′G is less constrained, but mainly 2′-endo. The two guanine bases result as strongly destacked, suggesting that if this feature is maintained in double-stranded DNA a relevant distortion of the duplex, mainly consisting of bending, should occur (as in the case of cisplatin complexes).

The nature of the intermediate reaction product B was not studied in detail. The main feature of this complex appeared to be a highly symmetric disposition of the ligands around the metal center (see CD spectrum, relative position of the CH8 resonances, and absence of coalescence of DMSO methyl resonances at basic pH). At variance with the final compound A, the H1′ coupling constants of both the N7-coordinated guanines indicated a sugar puckering mainly 2′-endo. A structure in which one guanine is trans to the halogen ligand and one is trans to a DMSO ligand is proposed and could be derived from the kinetic trans effect of the halogen atom.

Finally the irreversible binding of *trans*-$RuX_2(DMSO)_4$ (X = Cl, Br) is likely to be responsible for the DNA damage and antitumor action of these complexes. On the other hand, the reversibility of the N7 monofunctional binding may justify the low host toxicity and also give a rationale for the administration route.

REFERENCES

Admiraal, G., van der Veer, J. L., de Graff, R. A. G.; den Hartog, J. H. J., & Reedijk, J. (1987) *J. Am. Chem. Soc. 109*, 592–594.

Alessio, E., Attia, W. M., Calligaris, M., Cauci, S., Dolzani, L., Mestroni, G., Monti-Bragadin, C., Nardin, G., Quadrifoglio, F., Sava, G., Tamaro, M., & Zorzet, S. (1987) in *Platinum and Other Metal Coordination Compounds in Cancer Chemotherapy* (Nicolini, M., Ed.) pp 617–633, Martinus Nijhoff Publishing, Boston.

Alessio, E., Mestroni, G., Nardin, G., Attia, W. M., Calligaris, M., Sava, G., & Zorzet, S. (1988) *Inorg. Chem. 27*, 4099–4106.

Alessio, E., Xu, Y., Cauci, S., Mestroni, G., Quadrifoglio, F., Viglino, P., & Marzilli, L. G. (1989) *J. Am. Chem. Soc. 111*, 7068–7071.

Alessio, E., Balducci, G., Calligaris, M., Costa, G., Attia, W. M., & Mestroni, G. (1991) *Inorg. Chem. 30*, 609–618.

Altona, C. (1982) *Recl. Trav. Chim. Pays Bas 101*, 413–433.

Bau, R., & Gellert, R. W. (1978) *Biochimie 60*, 1040.

Bellon, S. F., Coleman, J. H., & Lippard, S. J. (1991) *Biochemistry 30*, 8026–8035.

Borgias, B. A., & James, T. (1988) *J. Magn. Reson. 79*, 493–512.

Cauci, S. (1990) Ph.D. Thesis, University of Trieste, Trieste, Italy.

Cauci, S., Viglino, P., Esposito, G., & Quadrifoglio, F. (1991) *J. Inorg. Biochem. 43*, 739–751.

Chaney, S. G., Gibbons, G. R., Wyrick, S. D., & Podhasky, P. (1991) *Cancer Res. 51*, 969–973.

Choi, H.-K., Huang, S. K.-S., & Bau, R. (1988) *Biochem. Biophys. Res. Commun. 156*, 1125–1129.

Clarke, M. J. (1989) *Prog. Clin. Biochem. Med. 10*, 25–39.

den Hartog, J. M. J., Altona, C., Chottard, J. C., Girault, J. P., Lallemand, J. Y., de Leeuw, F. A. A. M., Marcelis, A. T. M., & Reedijk, J. (1982) *Nucleic Acids Res. 10*, 4715–4730.

Drobny, G., Pines, A., Sinton, S., Weitekamp, D., & Wemmer, D. (1979) *Faraday Symp. Chem. Soc. 13*, 49–58.

Esposito, G., Gibbons, W. A., & Bazzo, R., (1987) *J. Magn. Reson. 80*, 523–527.

Fichtinger-Schepman, A. M. J., van der Veer, J. L., den Hartog, J. H. J., Lohman, P. H. M., & Reedijk, J. (1985) *Biochemistry 24*, 707–713.

Garzon, F. T., Berger, M. R., Keppler, B. K., & Schmahl, D. (1987) *Cancer Chemother. Pharmacol. 19*, 347–349.

Gasteiger, J., & Marsili, M. (1980) *Tetrahedron 36*, 3219–3228.

Girault, J. P., Chottard, G., Lallemand, J. Y., & Chottard, J. C. (1982) *Biochemistry 21*, 1352–1356.

Haasnot, C. A. G., de Leeuw, F. A. A. M., & Altona, C. (1980) *Tetrahedron 36*, 2783–2792.

Henn, M., Alessio, E., Mestroni, G., Calligaris, M., & Attia, W. M. (1991) *Inorg. Chim. Acta 187*, 39–50.

Jeener, J., Meier, B. H., Bachmann, P. & Ernst, R. R. (1979) *J. Chem. Phys. 71*, 4546–4553.
Johnson, N. P., Butour, J.-L., Villani, G., Wimmer, F. L., Defais, M., Pierson, V., & Brabec, V. (1989) *Prog. Clin. Biochem. Med. 10*, 1–24.
Karplus, M. (1959) *J. Chem. Phys. 30*, 11–15.
Kay, L. E., Holak, T. A., Johnson, B. A., Armitage, L. M., & Prestegard, J. H. (1986) *J. Am. Chem. Soc. 108*, 4242–4244.
Kirkpatrick, S., Gelatt, C. D., Jr., & Vecchi, M. P. (1983) *Science 220*, 671–680.
Kumar, A., Wagner, G., Ernst, R. R., & Wuthrich, K. (1981) *J. Am. Chem. Soc. 103*, 3654–3658.
Lankorst, P. P., Haasnot, C. A. G., Erkelens, C., & Altona, C. (1984) *J. Biomol. Struct. Dyn. 1*, 1387–1405.
Lippard, S. J. (1987) *Pure Appl. Chem. 59*, 731–742.
Loehrer, P. J., & Einhorn, L. H. (1984) *Ann. Intern. Med. 100*, 704–713.
Macura, S., Huang, Y., Suter, D., & Ernst, R. R. (1981) *J. Magn. Reson. 43*, 259–281.
Mercer, A., & Trotter, J. (1975) *J. Chem. Soc., Dalton Trans.* 2480–2483.
Mestroni, G., Alessio, E., Calligaris, M., Attia, W. M., Quadrifoglio, F., Cauci, S., Sava, G., Zorzet, S., Pacor, S., Monti-Bragadin, C., Tamaro, M., & Dolzani, L. (1989) *Prog. Clin. Biochem. Med. 10*, 71–87.
Miller, S. K., & Marzilli, L. G. (1985) *Inorg. Chem. 24*, 2421–2425.
Morris, G. A., & Freeman, R. (1978) *J. Magn. Reson. 29*, 433–462.
Muggia, F. M. (1991) *Semin. Oncol. 18*, 1–4.
Mukundan, S., Jr., Xu, Y., Zon, G., & Marzilli, L. (1991) *J. Am. Chem. Soc. 113*, 3021–3027.
Muller, L., & Ernst, R. R. (1979) *Mol. Phys. 38*, 963–992.
Orbell, J. D., Marzilli, L. G., & Kistenmaker, T. J. (1981) *J. Am. Chem. Soc. 103*, 5126–5133.
Pacor, S., Sava, G., Ceschia, V., Bregant, F., Mestroni, G., & Alessio, E. (1991) *Chem.-Biol. Interact. 78*, 223–234.
Piantini, U., Sorensen, O. W., & Ernst, R. R. (1982) *J. Am. Chem. Soc. 104*, 6800–6801.
Rance, M. (1987) *J. Magn. Reson. 74*, 557–564.
Reedijk, J. (1987) *Pure Appl. Chem. 59*, 181–192.
Remin, M., & Shugar, D. (1972) *Biochim. Biophys. Res. Commun. 48*, 636–641.
Rinkel, L. J., & Altona, C. (1987) *J. Biomol. Struct. Dyn. 4*, 621–649.
Saenger, W., (1984) in *Principles of Nucleic Acid Structure*, Chapters 2 and 4, Springer-Verlag, New York.
Sava, G., Pacor, S., Zorzet, S., Alessio, E., & Mestroni, G. (1989) *Pharmacol. Res. 21*, 617–628.
Seddon, E. A., & Seddon, K. R. (1984) in *The Chemistry of Ruthenium*, Elsevier, Amsterdam.
Shaka, A. J., Keeler, J., & Freeman, R. (1983) *J. Magn. Reson. 53*, 313–340.
Sherman, S. E., & Lippard, S. J. (1987) *Chem. Rev. 87*, 1153–1181.
Sherman, S. E., Gibson, D., Wang, A. H.-J., & Lippard, S. J. (1985) *Science 230*, 412–417.
Twelves, C. J., Ash, C. M., Miles, D. W., Thomas, D. G. T., & Souhami, R. L. (1991) *Cancer Chemother. Pharmacol. 27*, 481–483.
Weiner, J. S., Kollman, P. A., Case, D. A., Singh, U. C., Ghio, C., Alagona, G., Profeta, S., & Weiner, W. (1984) *J. Am. Chem. Soc. 106*, 765–784.
Weiss, G., Green, S., Alberts, D. S., Thigpen, J. T., Hines, H. E., Hanson, K., Pierce, H. I., Baker, L. H., & Goodwin, J. W. (1991) *Eur. J. Cancer 27*, 135–138.
Wuthrich, K. (1986) in *NMR of Proteins and Nucleic Acids*, Chapter 11, Wiley-Interscience, New York.